Applied Catalysis B: Environmental 126 (2012) 326–333

Contents lists available at SciVerse ScienceDirect

Applied Catalysis B: Environmental

journal homepage: www.elsevier.com/locate/apcatb

Degradation of methylene blue by catalytic and photo-catalytic processes catalyzed by the organotin-polymer $^{3}{}_{\infty}[(Me_3Sn)_4Fe(CN)_6]$

Safaa El-din H. Etaiw*, Mohamed M. El-bendary

Department of Chemistry, Faculty of Science, Tanta University, Tanta 31527, Egypt

ARTICLE INFO

Article history:
Received 2 May 2012
Received in revised form 12 July 2012
Accepted 31 July 2012
Available online 8 August 2012

Keywords:
Fenton and photo-Fenton reaction
Catalysis
Kinetics
Organotin-polymer
Methylene blue

ABSTRACT

The organotin-polymer $[(Me_3Sn)_4Fe(CN)_6]$, **1**, has been synthesized and characterized to test its potential application as catalyst. The structure of **1** consists mainly, of $[Fe(CN)_6]^{4-}$ building blocks connected by the Me_3Sn cations forming 3D-polymeric network. The iron (II) sites acquire distorted octahedral geometry while the tin atom exhibits TBPY-5 configured $[Me_3Sn(CN...)_2]$ fragments. Fenton and photo-Fenton oxidative discoloration of methylene blue (MB) has been investigated by hydrogen peroxide catalyzed with the metal–organic framework, (MOF) **1**. The reaction is first order with respect to MB dye. The irradiation of the reaction with UV-light enhanced the rate of MB mineralization. Mineralization of MB was investigated by FT-IR spectra. Disodium salt of terephthalic acid photoluminescence probing technology was carried out to identify the reactive oxygen species. The different parameters that affect MB degradation rate were evaluated. Moreover, the efficiency of recycled the catalyst **1** and the mechanism of degradation of MB dye were investigated.

1. Introduction

In the textile and food industries, the uses of organic dyes are the important sources of environmental contaminations due to their high toxicity to aquatic creatures and carcinogenic effects on humans [1,2]. The major issue related to these organic dyes in large quantities in wastewater is their chemical stability and low biodegradability in water systems, which is potentially harmful to the eco-environment. As a consequence, an effective and economic technique needs to be developed to reduce the concentrations of these contaminants before releasing the wastewater into the aquatic environment. In this concern, traditional physical techniques employed to remove such recalcitrant pollutants were found to be non-destructive, because they just transferred organic matter from water to sludge. This led to the requirement of regeneration of the adsorbent materials and post-treatment of solid wastes and both of them cost a lot [3]. On the other hand, several techniques such as adsorption, oxidation, reduction, photocatalysis and membrane filtration are usually applied to remove large organic pollutants from the industrial effluents. Among these techniques developed in wastewater treatment, advance oxidation processes (AOPs) are increasingly used as for the reduction of organic contaminants in a variety of wastewaters from different industrial plants. The widely used AOPs include photolysis, Fenton method, photo-Fenton, ozonolysis, sonolysis, and photo-catalysis [4–7]. The AOPs are usually driven by hydroxyl radicals produced in the system [8–10]. The advantage of AOPs is the conversion of organic compounds to less toxic molecules. In perfect conditions, it is possible to oxidize the organic molecules completely to CO_2 and H_2O. Currently, H_2O_2 is reported as an effective oxidant for the production of hydroxyl radicals. Among several AOPs, heterogeneous photo-oxidation is presented as a low cost effective procedure for removing stable organic compounds including dye molecules [11–13]. Heterogeneous photo-catalysts trigger the formation of oxidant radicals through low energy photon absorption. The other benefit of the heterogeneous photo-catalysis is the catalyst recycling that would minimize the use of the material and cost of the treatment [14].

The organometallic coordination polymers, and likewise potential epoxide polymerization catalysts, of the type $[(R_3E)_{3/4}M^{III/II}(CN)_6]$ where R = alkyl, Ph, E = Sn or Pb and M = Fe or Co may even share several of characteristic properties with zeolites [15–21]. The porous nature of these materials and/or the presence of possibly catalytically active transition-metal centers are seen as the basis of size- and shape-selective catalytic applications of such materials [22,23]. The organotin coordination polymer $[(Me_3Sn)_4Fe(CN)_6]$, **1** can be considered as a member of this rapidly growing class of porous materials containing organotin(IV) fragments and the $[M(CN)_6]$ building blocks. The lattice of these organotin polymers consists of octahedral $[M(CN)_6]^{n-}$ which are continuously interlinked by practically planar R_3Sn fragments creating 3D-network. The tin atoms became thus, five-coordinate, the cyanide N atoms occupying throughout the axial TBPY-5 positions [15–21].

* Corresponding author. Tel.: +20 1149442423; fax: +20 403350804.
E-mail address: safaaetaiw@hotmail.com (S.E.-d.H. Etaiw).

0926-3373/$ – see front matter © 2012 Elsevier B.V. All rights reserved.
http://dx.doi.org/10.1016/j.apcatb.2012.07.032

The use of such organotin polymers as heterogeneous catalytic systems should eliminate the needs of adding soluble catalytic substances. Transition metal complexes supported on different surfaces and metal–organic framework were used as potentially active catalysts for the decomposition of H_2O_2 and the oxidative degradation of organic contaminants and dyes [20–27].

Methylene blue (MB) is one of the most commonly used substances for dyeing cotton, wood and silk. It is potentially harmful to the eco-environment therefore the degradation of MB dye has attracted much attention [11,12,28]. The present work aims at studying the kinetics and mechanism of the oxidative discoloration of MB with H_2O_2 catalyzed by the coordination polymer **1**. The attractive properties of **1** as the wide surface area and the remarkably expandable channels which are capable to encapsulate organic compounds, allow it to be used as effective catalyst. This model system may be applicable to color removal in a textile waste water stream.

2. Experimental

2.1. Materials and working procedures.

The organotin polymer **1** was prepared according to the literature procedure [29]. A solution of 90 mg (0.31 mmol) of $K_4[Fe(CN)_6]$ in 10 mL H_2O was added, under gentle stirring to an aqueous solution of 189 mg (0.95 mmol) of Me_3SnCl. White crystalline powder started growing from the initially clear solution. After filtration, washing with small quantities of cold H_2O and overnight drying, 81 mg (52.4% referred to $K_4[Fe(CN)_6]$) of the white crystals were obtained. Elemental analysis data for **1** ($C_{18}H_{36}N_6FeSn_4$, M.W. = 867.13) are as follows, anal. Calcd: C, 24.93; H, 4.18; N, 9.69; Fe, 9.96. Found: C, 24.84; H, 4.06; N, 9.79; Fe, 9.87.

The dye under investigation namely methylene blue (MB), with a labeled purity of more than 90% was obtained from Sigma–Aldrich and used as such, Scheme 1. Deionized water was used to make the dye solutions of desired concentration. Hydrogen peroxide (30%) was obtained from Merck.

Microanalyses (C, H, N) were carried out with a PerkinElmer 2400 automatic elemental analyzer. The IR spectra were recorded on PerkinElmer 1430 Ratio Recording Infrared Spectrophotometer as KBr discs. Nuclear magnetic resonance spectra (^1H and ^{13}C) were recorded on a Bruker 600 MHz spectrometer at ambient temperature using DMSO-d_6 as solvent. The magnetic susceptibility was determined with a Super Megohmeter devised by D.F. Evans, Shimadzu (UV-3101 PC) spectrometer was used to monitor the changes of the dye absorbance during the reaction course. It is equipped with an electronically temperature control unit (TCC-260) to maintain constant temperature with an accuracy ± 0.1 °C. Fluorescence spectra were measured with a PerkinElmer (LS 50 B) spectrometer. A shaker water thermostat (Julabo SW20 C) was used to shake the heterogeneous reaction mixture at 120 rpm at fixed temperature ± 0.1 °C. The pH values of the solutions are adjusted using Crison pH-meter digit-501 that had been calibrated prior to the measurements. Total organic carbon (TOC) was measured by Total Carbon Analyzer Seiver 5310C. The H_2O_2 concentration was determined by iodometric titration where H_2O_2 oxidizes iodide to iodine in the presence of sulfuric acid and molybdate catalyst. The iodine formed is titrated with thiosulfate solution, incorporating a starch indicator.

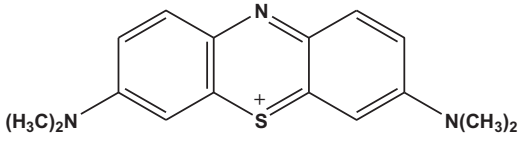

Scheme 1. Structure of methylene blue (MB).

2.2. Kinetic measurements

In typical kinetic run, a number of conical flasks (100 ml) containing a definite quantity of the solid catalyst together with the appropriate volume of distilled H_2O were placed in a water shaker thermostat in order to attain the desired temperature. To each conical flask, an appropriate volume of the separated thermostated dye and H_2O_2 solutions were added and zero time was noted. At regular time intervals aliquots of each conical flask were withdrawn and the absorbance was recorded at the corresponding λ_{max} of dye. In the absence of the catalyst, the dye/H_2O_2 mixture was stable for several hours without any noticeable change in the absorbance of dye, which indicates that no reaction takes place between the dye and H_2O_2. The photo-degradation experiments were carried out in a thermostated bath-type photo-reactor. (**1** + H_2O_2) was acted as photo-Fenton using UV light as illuminating light source. The light source is medium pressure mercury lamp (365 nm). Reaction system was setup by adding the photo-catalyst into 250 ml dye solution prepared in appropriate concentration using deionized water. The solution was stirred and 5 ml samples were withdrawn at regular time intervals and the dye concentrations were measured spectrophotometrically.

3. Results and discussion

3.1. Structure and characterization of the organotin-polymer *1*

The MOF **1** precipitates spontaneously from aqueous solution when solvated Me_3Sn^+ and $[Fe(CN)_6]^{4-}$ ions are brought together in the appropriate concentrations. The IR spectrum of the MOF **1** shows strong well resolved bands characteristic of the Me_3Sn units and the $[Fe(CN)_6]^{4-}$ fragments, Table 1 and Fig. 1. The two strong bands at 2072 and 2045 cm^{-1} correspond to $\upsilon_{C\equiv N}$. The appearance of these bands advocates the presence of two kinds of the cyanide ligands with different bond orders. This opinion is further supported by the appearance of two bands at 445 and 452 cm^{-1}

Table 1
The IR, NMR and electronic absorption spectra of the MOF **1**.

IR-spectra (cm^{-1})				NMR-spectra (ppm)		UV/vis spectra (nm)	
Band	Assignment	Band	Assignment	^1H	^{13}C	Band	Assignment
3095	υ_{CH}	1435	δ_{CH}	0.37	7.23	217	LMCT
3040		1380		0.55	7.84	248	MLCT
2072	υ_{CN}	793	γ_{CH}		169.12	310–330[b]	$\pi-\pi^*Fe^{II}$ (CN)
2045					178.44		
					174.91		
1580	$\upsilon_{C=C}$	592	υ_{Fe-C}				
1523		553	υ_{Sn-C}				
1498		452, 445	υ_{Sn-N}				

b = broad

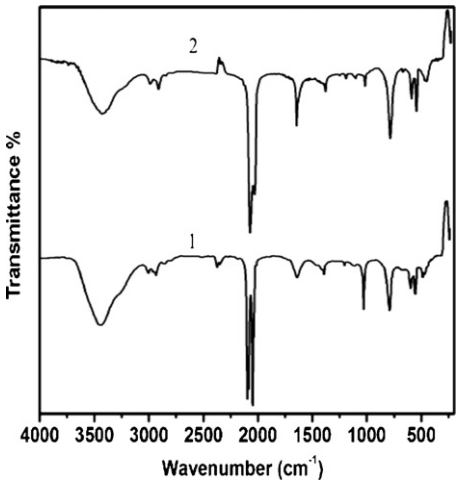

Fig. 1. IR spectra of the SCP catalyst **1**, 0.031 mM, before (1) and after (2) degradation of MB, 5×10^{-6} M, in presence of H_2O_2, 30 mM, at pH 6.

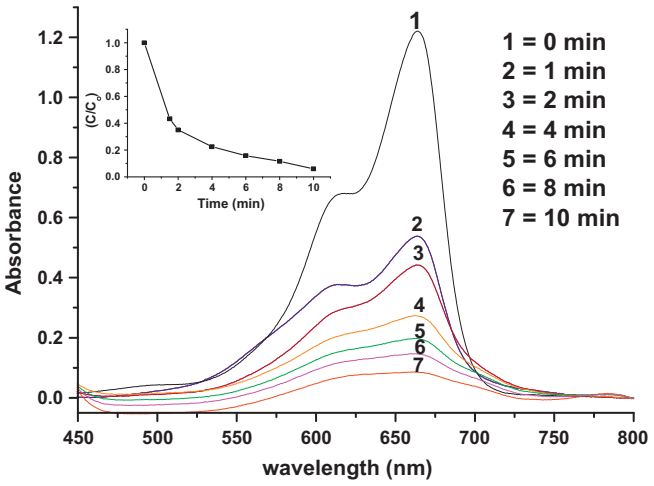

Fig. 2. Electronic absorption spectra of MB degradation with the MOF **1** in presence of MB 5×10^{-6} M, H_2O_2 30 mM and the MOF **1**, 0.031 mM at pH 6 and 30 °C.

due to υ_{Sn-N} indicating that one of the two different cyanide ligands connect one iron atom and one tin atom while the carbon end of the other cyanide ligand is free [30,31]. The band at 592 cm^{-1} is due to υ_{Fe-C} while the presence the asymmetric υ_{Sn-C} band at 553 cm^{-1} reflects the formation of the trigonal bipyramid (TBPY-5) configured Me_3SnN_2 connecting units in the network structure of **1**. The characteristic bands of the methyl ligands appear at the usual wave numbers, Table 1. On the other hand, the protons of the Me_3Sn units give rise to absorption indicated by the two peaks at 0.37 and 0.55 ppm. The peaks of the Me_3Sn units in the spectrum of **1** suffer upfield shift relative to those of Me_3SnCl (0.9 ppm) supporting participation of the Me_3Sn fragments in the structure of **1** as connecting units. The ^{13}C NMR spectrum of the MOF **1** shows the signals corresponding to the Me_3Sn and the cyanide ligands, Table 1. The Me_3Sn fragment absorbs at 7.23 and 7.84 ppm. The cyanide region has three signals at 169.12, 174.91 and 178.44 ppm, probably due, in part to second order effects arising from dipolar coupling to the quadrupolar ^{14}N nucleus [17] and to the presence of μ_2-cyanide ligands [17,32]. Although single crystals of the strictly anhydrous MOF **1,** could not be obtained so far, the asymmetric unit of **1** as well as the local symmetries of the Me_3Sn and $[Fe(CN)_6]$ building blocks have been unambiguously deduced from detailed CPMAS solid-state NMR and infrared/Raman spectroscopic studies [17]. Also, the crystal structure of the zeolite-like host-guest networks were found for $[(Ph_3Sn)_3Fe(CN)_6{\cdot}H_2O{\cdot}2CH_3CN]$, **2** [16], $[(Me_3Sn)_4Fe(CN)_6{\cdot}2H_2O{\cdot}C_4H_8O_2]$, **3**, [29] and$[(Me_3Sn)_4Fe(CN)_6{\cdot}4H_2O]$, **4** [32]. The structures of the SCP **2**, **3** and **4** suggested the formation of host–guest systems. Their structures indicated the presence of octahedral $[Fe(CN)_6]_{3/4}$ building blocks connected by the TBPY-5 configured $Me_3Sn(CN\ldots)_2$ fragments as well as the presence of the quasi-mobile Me_3Sn^+ ions [12,16,18]. The networks consist of three chains which define stuffed channels down different axes [16]. From all spectroscopic findings, a three-dimensional network reminiscent of that of the polymeric acid $[H_4Fe(CN)_6]$ may be deduced [17]. Thus, the elemental analysis and spectroscopic results of the MOF **1** indicated the chemical composition $[(Me_3Sn)_4Fe(CN)_6]$. The octahedral $[Fe(CN)_6]^{4-}$ building blocks are connected by the TBPY-5 configured $Me_3Sn(CN)_2$ fragments creating 3D-network structure containing terminal cyanide groups.

The absorption spectrum of the MOF **1** exhibits bands at 217, 248 and 310–330 nm, Table 1. The broad band at 310–330 nm can be attributed to π–π^* transitions within the $[Fe^{II}(CN)_6]$ fragment [33] which is similar to the band at 320 nm in the spectrum of $K_4[Fe(CN)_6]$. The two bands at 217 and 248 nm are due to LMCT and MLCT, respectively within the $[Fe^{II}(CN)_6]$ building blocks [33].

3.2. Catalytic and photo-catalytic degradation of MB dye

Representative UV–vis spectra changes observed during MB degradation by the heterogeneous catalyst **1** in the presence of H_2O_2 are depicted in Fig. 2. The spectrum of MB exhibits three major absorbance bands at 250, 296 and 664 nm, due to π–π^* transitions of the benzene ring and hetero- polyaromatic linkage and to CT, respectively. These three absorbance peaks became weaker and weaker in intensity as the treatment time prolong. After 20 min, these three peaks almost totally disappeared, which indicated the benzene ring and hetero-polyaromatic linkage of methylene blue were almost destroyed. This indicates that the MB dye was nearly degraded completely into its mineral components. The insert in Fig. 2 shows lineal decreasing of absorbance at 664 nm during the first 2 min and then exponential. This behavior was also observed for other H_2O_2-based degradation systems [34], which can be explained by the fact, that the formation of the catalytic active species is the rate-determining step.

The rate of the catalytic oxidation of MB was studied using H_2O_2 as oxidant and **1** as heterogeneous catalyst. When a solution of MB was mixed with hydrogen peroxide, no reaction was observed. Also, no changes in the absorption spectrum of MB have been observed under photolysis indicating that photolysis alone is unable to degrade the MB dye, S 1. However, when the catalyst **1** is added, a reaction takes place leading to a color removal of the dye. The observed rate constant, k_{obs}, was determined from the slope of the first-order plot which verifies Eq. (1).

$$\ln A_t = \ln A_0 - k_{obs} \cdot t \quad \text{or} \quad \ln \frac{A_0}{A_t} = k_{obs} \cdot t \tag{1}$$

A_t is the absorbance at time = t and A_0 is the absorbance at $t = 0$. The plot indicates pseudo first- order rate with respect to the MB dye concentration ($k_{obs} = 0.28\ min^{-1}$), Fig. 3. The specific rate constant k was determined from the relation $k = k_{obs}/[MOF]$ which equals to 9.03 L/mol min.On the other hand, the photo-catalytic degradation of MB dye was investigated under the same conditions used for the catalytic degradation. The solution was subjected to UV light and the change in the absorption spectra of the dye solution was monitored at regular intervals of time. It was noted that the absorption value of MB dye became less with irradiation time, thus indicating the decolorization of MB dye solution ($k_{obs} = 0.33\ min^{-1}$). The decrease in absorption value of dye solution can be related in terms

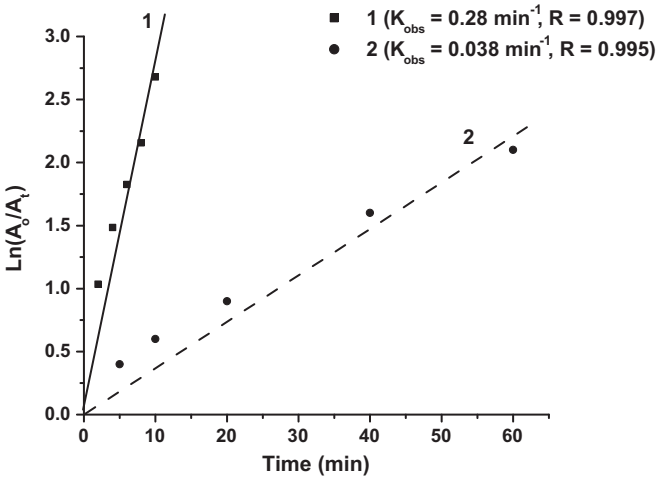

Fig. 3. Kinetic of degradation of MB, 5×10^{-6} M and the MOF **1**, 0.031 mM, in the presence (1) and the absence (2) of H_2O_2, 30 mM at pH 6 and 30 °C.

of the degradation efficiency (R_{color}), Fig. 4, which was evaluated by using the following relationship [3]:

$$R_{color}(\%) = A_0^{\lambda max} - \frac{A_t^{\lambda max}}{A_0^{\lambda max}} \times 100\%$$

where A_0 represents the initial absorbance of dyes solution and A_t represents the absorbance of the dye at time t. The specific rate constant k equals to 13.32 L/mol min indicating that irradiation enhances, significantly, the rate of degradation of MB dye. On the other hand, the kinetic data were determined by the method of initial rates by monitoring the decrease in absorbance of the band at 664 nm of MB due to aerobic oxidation in the presence of catalyst **1**, Figs. 3 and 5. The color disappears completely after 3 h while the insert in Fig. 5 shows lineal decreasing of absorbance at 664 nm during the first 10 min and then exponential (k_{obs} = 0.038 min^{-1}). The specific rate constant k equals to 1.22 L/mol min indicating efficient catalysis of **1** in absence of H_2O_2 in spite of the fact that the rate of degradation is slower.

See S 1 as supplementary file. Supplementary material related to this article found, in the online version, at http://dx.doi.org/10.1016/j.apcatb.2012.07.032.

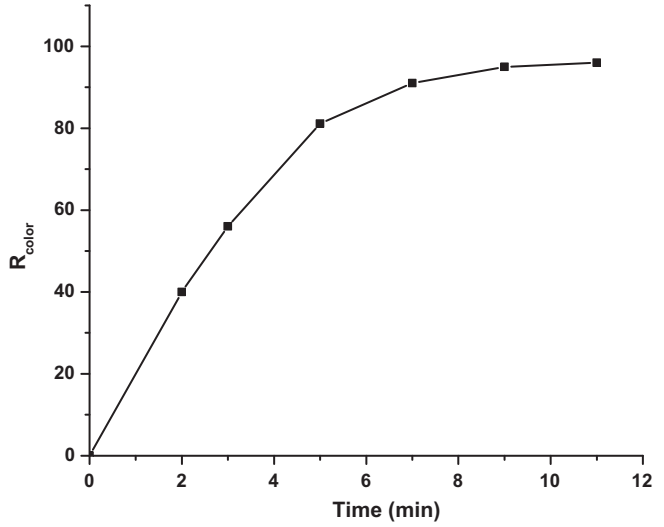

Fig. 4. The degradation efficiency of MB as a function of time.

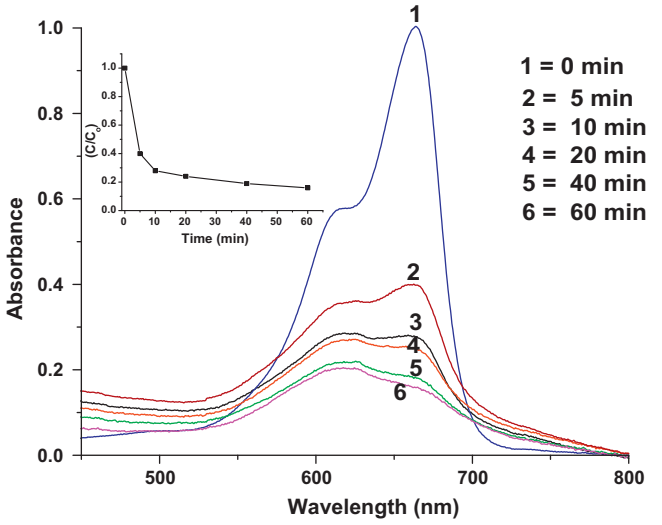

Fig. 5. Electronic absorption spectra of MB degradation with the MOF **1**in presence of MB 5×10^{-6} M, and the catalyst 0.031 mM at pH 6 and 30 °C.

3.3. Recyclization of the catalyst

An important issue that must be addressed while studying liquid-phase oxidations over a solid catalyst is a possibility of catalyst recycling. In each case, after the end of the first experiment, the catalyst is washed with double distilled water, dried, and then starting a new experiment. It was found that the catalyst **1** maintained its catalytic activity for two cycles of the dye oxidation with hydrogen peroxide. After the second cycle, the catalytic activity decreases. The IR spectra, Fig. 1, display no change in the region of the cyanide group stretching vibrations upon recyclization which indicates that the catalyst was not oxidized by H_2O_2, the case which was further supported by elemental analyses. The decrease in the efficiency of the catalyst **1** upon recyclization may be attributed to the poisoning of this catalyst by the oxidation products. Also, magnetic susceptibility measurements reveal that **1** is still diamagnetic which indicates that the structure of the catalyst **1** after the catalytic cycles remains containing the $Fe^{II}(CN)_6$ building blocks.

3.4. Hydroxyl radical determination

In order to identify the reactive oxygen species formed in the catalyst **1**/H_2O_2−system, disodium salt of terephthalic acid (NaTA) photoluminescence probing technology and radical scavenging measurements were carried out. NaTA could react with •OH to give 2-hydroxy terephthalic acid (HTA), which exhibits a bright stable fluorescence [35]. This reaction is unaffected by the presence of other reactive species such as H_2O_2, HO_2• and O_2•−, so it could be used as a sensitive probe in detecting •OH radicals [36]. Fig. 6 shows the fluorescence spectra of the solution containing the catalyst **1**/H_2O_2–system and NaTA. It can be seen that the fluorescence intensity increases sharply to 1000 within 10 min, implying that •OH radicals were indeed generated in the system. Moreover, when MB and NaTA were simultaneously added into the solution, the generated fluorescence significantly decreased, with the intensity only increasing to 250 within 30 min, Fig. 7.The main reason may be that part of •OH radicals reacted rapidly with MB, as the decolorization was observed during fluorescence measurement. Recently, the •OH radicals produced on various semiconductor photo-catalysts in aqueous solution under Xenon lamp irradiation were quantitatively investigated by the photoluminescence (PL) technique using

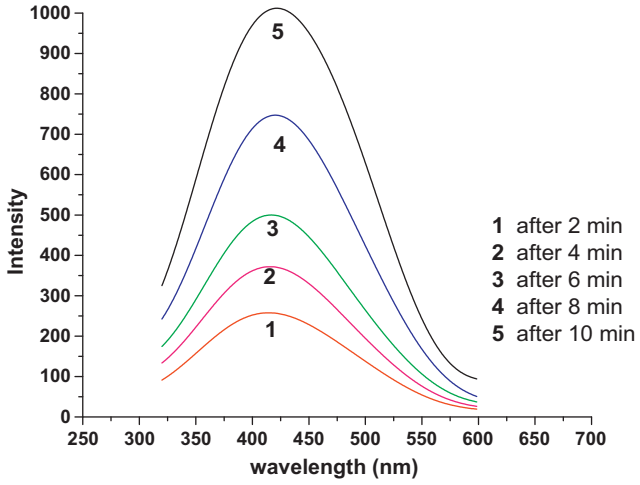

Fig. 6. Photoluminescence spectra of the MOF catalyst **1**, 0.031 mM, NaTA, 0.15 mM and H_2O_2, 30 mM at pH 6 as function of time.

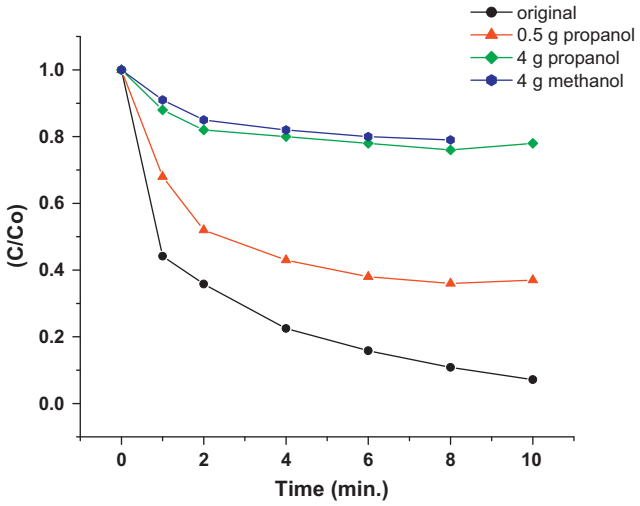

Fig. 8. Inhibited effects of 2-propanol and methanol on MB degradation.

coumarin as a probe molecule [37]. The amount of the •OH radicals produced by the present photo-Fenton reaction could be compared with that produced by anatase TiO_2 and Degussa P25 (P25) [37]. However, the addition of the present catalyst (MOF **1**) to the "OH-index" should be conducted in future work. On the other hand, the inhibited effects of 2-propanol and methanol, which are known to be effective scavenging agents for hydroxyl radicals [38,39], were also measured. As shown in Fig. 8, the rate of MB degradation became slower at relatively low concentration of 2-propanol; while at high concentrations of 2-propanol and methanol, great inhibition was observed indicating that the hydroxyl radicals are the major active species during the photo-catalytic oxidation reaction.

3.5. Degradation products analyses

The products remained in solution after MB complete degradation by the catalyst **1** and H_2O_2 were monitored by FT-IR spectra and absorption spectroscopy. Fig. 9 shows the FT-IR spectra of MB before and after degradation. Prior to degradation, MB exhibited the prominent bands of the characteristic C=N central ring stretching vibrations at 1599 cm^{-1}, C=C side ring stretching vibrations at 1537 and1482 cm^{-1}, multiple ring stretching vibrations at 1394 cm^{-1}, C_{Ar-N} (the bond between the side aromatic ring and the nitrogen atom) stretching vibrations at 1345 cm^{-1}, and N—CH_3 stretching vibrations at 1240 and 1184 cm^{-1} [40]. After treatment by the catalyst **1** and H_2O_2, the disappearance of the above-mentioned characteristic bands indicated complete destruction of MB molecule by breaking of central and side aromatic rings as well as demethylation. Meanwhile, three new intense peaks at 1450, 1380 and 1224 cm^{-1} appeared, which might be due to the stretching vibrations of COO^-, NO_3^- and SO_4^{2-}, respectively [40], suggesting that the carbon dioxide is the main final product in addition to some acids. The complete oxidative degradation of the dye led to the conversion of organic carbon into gaseous CO_2 which was trapped by $Ca(OH)_2$ solution and the precipitated $CaCO_3$ was determined gravimetrically. Also, the percentage degree of the total organic carbon (TOC) in the sample was carried out. This measurement shows that about 92% of the MB dye was degraded completely into its mineral components after about 30 min.

Methylene blue (MB) shows one main band in the visible region, with its maximum absorption at 665 nm with a small

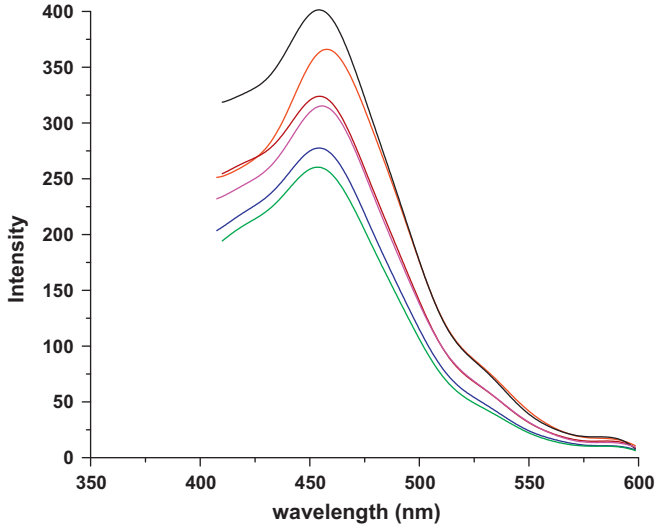

Fig. 7. Photoluminescence spectra of the MOF catalyst **1**, 0.031 mM, MB 5×10^{-6} M,H_2O_2, 30 mM and NaTA, 0.15 mM at pH 6 as function of time (every 5 min).

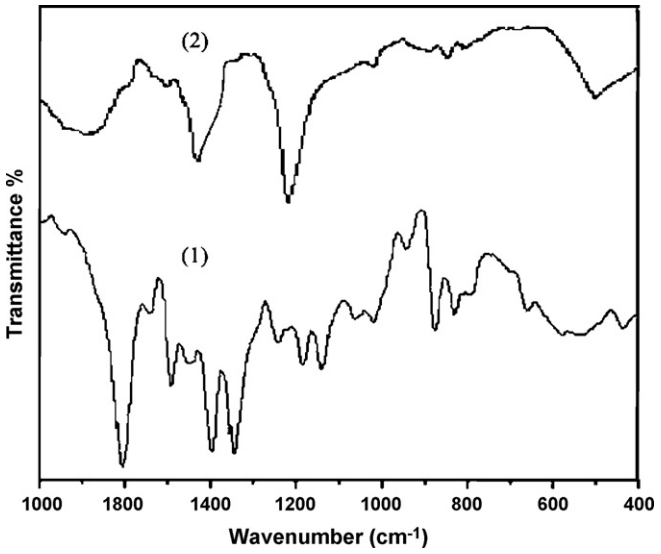

Fig. 9. IR spectra of MB before (1) and after (2) degradation.

shoulder at 615 nm and two bands in the ultraviolet region located at 245 and 296 nm. The conjugation system between the two dimethylamine substituted aromatic rings through the sulfur and nitrogen is responsible for the absorbance at 665 nm, while the small shoulder at 615 nm has been reported due to the absorbance of the dye dimmer [41,42]; whereas, the substituted benzene rings have their $^1L_a \leftarrow {}^1A$ and $^1L_b \leftarrow {}^1A$ absorption bands in the ultraviolet region. It was clearly observed that the absorption peaks at 615 and 665 nm diminished very fast. This indicated a rapid degradation of MB and the destruction of the aromatic system.

3.6. Effect of operational parameters on MB dye degradation

For the degradation experiments, many factors affect the degradation efficiency, such pH, the concentration of dye, scavenging agents, anions, catalyst dosage and reaction temperature, etc. To optimize design of an existing process, it is necessary to identify which factors have the greatest influence and which values produce the most consistent performance. Thus, the effect of dye concentration, catalyst amount, pH effect and photo-radiation has been reported for various dye degradation studies [43,44]. These parameters were also studied in the present case and the results are shown in Table 2. Initial MB dye concentrations were set in the range of 1.0×10^{-6} to 1.0×10^{-5} M in presence of 0.1 M H_2O_2 and 0.025 mmol of the catalyst **1** at pH 5.5. Initially, a large degree of removal is observed. This is due to fast decomposition of H_2O_2 producing the hydroxyl radicals. Taking into account that, the lifetime of hydroxyl radical is very short (only few nanoseconds), they can only react where they are found [45]. Increasing the MB dye concentration leads to decrease in the degradation rate, Table 2. However, even at a high concentration of the MB dye; 1×10^{-5} M, complete decolorization was also observed after 110 min. The presumed reason is that, at high dye concentration, the generation of the $^{\bullet}OH$ radicals on the surface of catalyst is reduced since the active sites are covered by the dye ions. Thus, as the initial concentration of the dye is increased, the requirement of catalyst surface needed for degradation should be also increased.

The effect of catalyst concentration is an important parameter that can affect the degradation rate. By varying the amount of catalyst from 0.025 to 0.058 mmol, the rate of degradation increases, Table 2. It is evident that the catalyst surface is one of the limiting factors affecting the enhancement of the degradation rate. The increase in the amount of catalyst weight increases the number of the $^{\bullet}OH$ radicals.

The effect of varying the initial H_2O_2 concentration from 10 mmol to 60 mmol is investigated using dye concentration 5.0×10^{-6} M at pH 6. The initial H_2O_2 concentration strongly modifies the rates of degradation of MB, Table 2. At low H_2O_2 concentrations, formation of the $^{\bullet}OH$ radicals is the kinetic determining step. An increase in the H_2O_2 concentration up to 30 mmol leads to a dramatic rise in the solution discoloration rate. On the other hand, further increase in the H_2O_2 concentration partly inhibits the oxidation rate. This behavior is proof of the existence of an optimal dosage in H_2O_2. In the presence of high concentration of H_2O_2, more $^{\bullet}OH$ radicals would be produced which preferentially react with the excess of H_2O_2. This undesirable reaction competes with the destruction of the dye chromophore [46].

$$^{\bullet}OH + MB \rightarrow \text{oxidation products}$$

$$^{\bullet}OH + H_2O_2 \rightarrow HO_2{}^{\bullet -} + H_2O$$

In addition, pH was another factor which affected the discoloration efficiency of the MB dye. The effect of pH on the reaction rate was studied at constant concentrations of the dye and H_2O_2 as well as a fixed amount of the catalyst at 25 °C, Table 2. The results show that high degradation rate was observed at pH 6. At higher pH values, the degradation rate decreased gradually. In acidic media, the deprotonation of H_2O_2 is increased with the increase of pH, which should increase in the decomposition rate of H_2O_2 [47] leading to facile formation of the $^{\bullet}OH$ radicals. In alkaline medium, the oxidizing species; hydroperoxy anion ($HO_2{}^-$) which is the conjugate base of H_2O_2 is also formed. This $HO_2{}^-$ anion can react with the non- dissociated molecules of H_2O_2 which leads to oxygen and water [48].

$$H_2O_2 + HO_2{}^- \rightarrow H_2O + O_2 + OH^-$$

Furthermore, the deactivation of $^{\bullet}OH$ is greater when the pH of the solution is high [49]. The reaction of $^{\bullet}OH$ and $HO_2{}^-$ is approximately 100 times faster than its reaction with H_2O_2.

$$^{\bullet}OH + HO_2{}^- \rightarrow H_2O + O_2$$

On the whole, the results demonstrate that it is very important to set a suitable dye concentration, catalyst amount, initial H_2O_2 concentration and pH in order to optimize the operating conditions.

3.7. Fenton and photo-Fenton processes

The Fenton's reagent involves reaction of ferrous ions with hydrogen peroxide to produce hydroxyl radicals, which are strong oxidizing reagents that react with the dye solution causing its degradation [43,50].

$$H_2O_2 + Fe^{2+} \rightarrow {}^{\bullet}OH + OH^- + Fe^{3+} \quad (1)$$

Table 2
Catalytic degradation rates of MB in presence of different parameters.

Parameters [MB]/M	$k\,(min^{-1}) \times 10^2$	R	Parameters [H_2O_2]/mM	$k\,(min^{-1}) \times 10^2$	R
1×10^{-6}	35	0.983	10	15.7	0.988
5×10^{-6}	28	0.997	20	19.8	0.990
7×10^{-6}	21	0.995	30	28	0.997
1×10^{-5}	13.6	0.996	40	21.6	0.992
			60	13.2	0.983
[MOF 1]/mM	$k\,(min^{-1}) \times 10^2$	R	pH	$k\,(min^{-1}) \times 10^2$	R
0.025	28	0.997	4	24.8	0.995
0.040	36.2	0.996	5	26.3	0.995
0.05	48.6	0.989	5.5	27.2	0.998
0.058	57	0.992	6	28	0.972
			7.5	18.6	0.992

The hydroxyl radical propagates the reaction by reacting with MB dye to produce further radicals, which can then react in many different steps.

$$^{\bullet}OH + MB \rightarrow H_2O + MB^{\bullet} \quad (2)$$

$$MB^{\bullet} + H_2O_2 \rightarrow MB{-}OH + {}^{\bullet}OH \quad (3)$$

Additionally, many other reactions are also, possible which include the radical–radical reaction or the reaction of the $^{\bullet}OH$ with H_2O_2.

$$^{\bullet}OH + {}^{\bullet}OH \rightarrow H_2O_2 \quad (4)$$

$$^{\bullet}OH + H_2O_2 \rightarrow HO_2{}^{\bullet-} + H_2O \quad (5)$$

The peroxide radicals ($HO_2{}^{\bullet-}$) produced in the above case can further oxidize other species present in the solution [51].

$$HO_2{}^{\bullet-} + Fe^{2+} \rightarrow O_2 + Fe^{3+} + H^+ \quad (6)$$

However, the reactivity of $HO_2{}^{\bullet-}$ and its basic form $O_2{}^{\bullet-}$ with organic compounds is very weak. They are preferentially disproportionate producing hydrogen peroxide and oxygen [52].

$$HO_2{}^{\bullet-} + O_2{}^{\bullet-} + H_2O \rightarrow H_2O_2 + O_2 + {}^{-}OH \quad (7)$$

The rapid depletion of H_2O_2 that is often observed with Fenton's reagents, is probably due to the combined reactions (1–6). This is supported by measuring the concentration of H_2O_2 consumed in Fenton reaction which equals to 4.6 mM based on the difference between the concentration of H_2O_2 in blank and in the presence of MB and catalyst. However, since reaction (2) has the highest rate constant; it is possible for Fe^{2+} to be auto regenerated in this system, and acts as a catalyst [53].

$$Fe^{3+} + H_2O_2 \rightarrow Fe^{2+} + H^+ + HO_2{}^{\bullet} \quad (8)$$

On the other hand, the increase in rate of degradation of MB dye on irradiation is due to the enhancement of the production of the hydroxyl radicals which are generated upon photolysis of hydrogen peroxide [44], following the reaction:

$$H_2O_2 + h\upsilon \rightarrow 2{}^{\bullet}OH \quad (9)$$

In this case the consumption of H_2O_2 increases (8 mM) producing more hydroxyl radicals due to photolysis of hydrogen peroxide.

4. Conclusion

The MOF **1** can be considered as an efficient heterogeneous catalyst for elimination of MB in aqueous solution with H_2O_2. Similar to Fenton reagent, the system can produce hydroxyl radicals, as confirmed by photoluminescence probing and radical scavenging measurements. The irradiation of the reaction with UV-light enhanced significantly the rate of MB mineralization. This method is simple and does not involve any stringent reaction conditions. This method is a good alternative for the reported costly instrumental procedures [54], the electrochemical methods using silver electrode [55], or the photo-degradation methods using different catalysts like Ag–TiO_2 nanoparticles, elemental iron/MnO_2 system, Fe–fullerene/TiO_2 compounds, Ti–10Cr catalyst [54–59] and the SCP [$(ph_3Sn)_4Fe(CN)_6$] [60].

References

[1] G. Liu, X. Li, J. Zhao, H. Hidaka, N. Serpone, Environmental Science and Technology 34 (2000) 3982–3990.
[2] G.L. Baughman, E.J. Weber, Environmental Science and Technology 28 (1994) 267–276.
[3] S. Ameen, M.S. Akhtar, Y.S. Kim, O-B. Yang, H.-P. Cooper, Journal of the Society of Dyers and Colourists 109 (1993) 97–100.
[4] M.M. Alnuaimi, M.A. Rauf, S.S. Ashraf, Dyes and Pigments 72 (2007) 367–371.
[5] J.H. Sun, S.P. Sun, G.L. Wang, L.P. Qiao, Dyes and Pigments 74 (2007) 647–652.
[6] D.H. Bremner, R. Molina, F. Mart nez, J.A. Melero, Y. Segura, Applied Catalysis B: Environmental 90 (2009) 380–388.
[7] G. Moussavi, M. Mahmoudi, Chemical Engineering Journal 152 (2009) 1–7.
[8] D. Bahnemann, Solar Energy 77 (5) (2004) 445–459.
[9] C. Comninellis, A. Kapalka, S. Malato, S.A. Parsons, I. Poulios, D. Mantzavinos, Journal of Chemical Technology and Biotechnology 83 (6) (2008) 769–776.
[10] D.Y. Goswamee, S. Vijayaraghavan, S. Lu, G. Tamm, Solar Energy 76 (2001) 33–43.
[11] I. Fatimah, S. Wang, D. Wulandari, Applied Clay Science 53 (2011) 553–560.
[12] N. Liu, G. Sun, Dyes and Pigments 91 (2011) 215–224.
[13] A. Xu, X. Li, S. Ye, G. Yin, Q. fuZeng, Applied Catalysis B: Environmental 102 (2011) 37–43.
[14] H. Kusic, N. Koprivanac, L. Srsan, Journal of Photochemistry and Photobiology A181 (2006) 195–202.
[15] P. Schwarz, E. Siebel, R.D. Fischer, D.C. Apperley, N.A. Davies, R.K. Harris, Angewandte Chemie International Edition in English 34 (1995) 1197–1199.
[16] J. Lu, W.T.A. Harrison, A.J. Jacobson, Angewandte Chemie International Edition in English 34 (1995) 2557–2559.
[17] S. Eller, P. Schwarz, A.K. Brimah, R.D. Fischer, D.C. Apperley, N.A. Davies, R.K. Harris, Organometallics 12 (1993) 3232–3240.
[18] A.K. Brimah, E. Siebel, R.D. Fischer, N.A. Davies, D.A. Apperley, R.K. Harris, Journal of Organometallic Chemistry 475 (1994) 85–95.
[19] C. Carini, C. Pelizzi, G. Pelizzi, G. Predieri, P. Tarasconi, F. Vitali, Journal of the Chemical Society, Chemical Communications (1990) 613–614.
[20] J. Lu, W.T.A. Harrison, A.J. Jacobson, Inorganic Chemistry 35 (1996) 4271–4273.
[21] E. Siebel, R.D. Fischer, N.A. Davies, D.C. Apperley, R.K. Harris, Journal of Organometallic Chemistry 604 (2000) 34–42.
[22] M. Fujita, Y.J. Kwon, S. Washizu, K. Ogura, Journal of the American Chemical Society 116 (1994) 1151–1152.
[23] S. Hasegawa, S. Horike, R. Matsuda, S. Furukawa, K. Mochizuki, Y. Kinoshita, S. Kitagawa, Journal of the American Chemical Society 129 (2007) 2607–2614.
[24] I.A. Salem, Applied Catalysis B: Environmental 28 (2000) 153–166.
[25] S.E.H. Etaiw, A.S. Elsherbiny, A.S. Badr El-din, Chinese Journal of Chemistry 29 (2011) 1401–1410.
[26] R.G. El-sharkawy, A.S. Badr El-din, S.E.H. Etaiw, Spectrochimica Acta, Part A 79 (2011) 1969–1975.
[27] R.L. Valentine, H.C.A. Wang, Journal of Environment Engineering 124 (1998) 31–38.
[28] N. Talebian, M.R. Nilforoushan, Thin Solid Films 518 (2010) 2210–2215.
[29] M. Adam, A.K. Brimah, R.D. Fischer, L.X. Fu, Inorganic Chemistry 29 (1990) 1595–1597.
[30] C. Apperley, N.A. Davies, R.K. Harris, A.K. Brimah, S. Eller, R.D. Fischer, Organometallics 9 (1990) 2672–2676.
[31] U. Behrens, A.K. Brimah, T.M. Soliman, R.D. Fischer, D.C. Apperley, N.A. Davies, R.K. Harris, Organometallics 11 (1992) 1718–1726.
[32] U. Behrens, A.K. Brimah, R.D. Fischer, Journal of Organometallic Chemistry 411 (1991) 325–330.
[33] S.E.H. Etaiw, A.M.A. Ibrahim, Journal of Organometallic Chemistry 522 (1996) 77–86.
[34] A. Theodoridis, J. Maigut, R. Puchta, E.V. Kudrik, R. van Eldik, Inorganic Chemistry 47 (2008) 2994–3013.
[35] J.G. Yu, Q.J. Xiang, M.H. Zhou, Applied Catalysis B 90 (2009) 595–602.
[36] M. Sahni, B.R. Locke, Industrial and Engineering Chemistry Research 45 (2006) 5819–5825.
[37] Q. Xiang, J. Yu, P.K. Wong, Journal of Colloid and Interface Science 357 (2011) 163–167.
[38] S. Kim, W. Choi, Environmental Science and Technology 36 (2002) 2019–2025.
[39] Y.P. Huang, W.H. Ma, J. Li, M.M. Cheng, J.C. Zhao, Journal of Physical Chemistry B 107 (2003) 9409–9414.
[40] Z.Q. Yu, S.S. Chuang, Journal of Physical Chemistry B 111 (2007) 13813–13820.
[41] A.E.H. Machado, J.A. de Miranda, R.F. de Freitas, E.T.F.M. Duarte, L.F. Ferreira, Y.D.T. Albuquerque, R. Ruggiero, C. Sattler, L. de Oliveira, Journal of Photochemistry and Photobiology A: Chemistry 155 (2003) 231–241.
[42] C. Yogi, K. Kojima, N. Wada, H. Tokumoto, T. Takai, T. Mizoguchi, H. Tamiaki, Thin Solid Films 516 (2008) 5881–5884.
[43] A. Syoufian, K. Nakashima, Journal of Colloid and Interface Science 317 (2008) 507–512.
[44] H.Y. Shu, M.C. Chang, H.J. Fan, Journal of Hazardous Materials 113 (2004) 201–208.
[45] C. Galindo, P. Jacques, A. Kalt, Journal of Photochemistry and Photobiology A: Chemistry 141 (2001) 47–56.
[46] C. Galindo, A. Kalt, Dyes and Pigments 40 (1998) 27–35.
[47] I.A. Salem, R.I. El hag, K.M.S. Khalil, Transition Metal Chemistry 25 (2000) 260–264.
[48] M.P. Titus, V.G. Molina, M.A. Banos, J. Gimenez, S. Esplugus, Applied Catalysis B: Environmental 47 (2004) 219–256.
[49] S.G. Schrank, J.N.R. Santos, D.S. Souza, E.E.S. Souza, Journal of Photochemistry and Photobiology A: Chemistry 186 (2007) 125–129.
[50] X. Zhou, J. Lan, G. Liu, K. Deng, Y. Yang, G. Nie, J. Yu, L. Zhi, Angewandte Chemie International Edition 51 (2012) 178–182.
[51] W. Bae, S.H. Lee, G.B. Ko, Water Science and Technology 49 (4) (2004) 91–96.
[52] M.S. Khehra, H.S. Saini, D.K. Sharma, B.S. Chadha, S.S. Chimni, Water Research 39 (20) (2005) 5135–5141.
[53] E.G. Solozhenko, N.M. Soboleva, V.V. Goncharuk, Water Research 29 (1995) 2206–2210.

[54] C. Noubactep, G. Meinrath, P. Dietrich, M. Sauter, B. Merkel, Environmental Chemistry 2 (2005) 71–76.
[55] S.H. de AraujoNicolia, P.R.P. Rodrigues, S.M.L. Agostinho, J.C. Rubim, Journal of Electroanalytical Chemistry 527 (2002) 103–111.
[56] Y. Li, M. Ma, W. Chen, L. Li, M. Zen, Materials Chemistry and Physics 129 (2011) 501–505.
[57] C. Noubactep, Journal of Hazardous Materials 168 (2009) 1613–1616.
[58] Z.D. Meng, W.C. Oh, Ultrasonics Sonochemistry 18 (2011) 757–764.
[59] M.A. Rauf, M.A. Meetani, A. Khaleel, A. Ahmed, Chemical Engineering Journal 157 (2010) 373–378.
[60] A.M.A. Ibrahim, S.M.A. Al-Ashqar, Spectrochimica Acta, Part A 92 (2012) 238–244.